





Article

Preparation and Characterization of Shell-Based CaO Catalysts for Ultrasonication-Assisted Production of Biodiesel to Reduce Toxicants in Diesel Generator Emissions

Ngee S. Chong, Ifeanyi Nwobodo, Madison Strait, Dakota Cook, Saidi Abdulramoni and Beng G. Ooi

Special Issue

Advancements in Catalytic Conversion of Biomass into Biofuels and Chemicals II

Edited by

Prof. Dr. Tae Hyun Kim and Dr. A.V.S.L. Sai Bharadwaj









Article

Preparation and Characterization of Shell-Based CaO Catalysts for Ultrasonication-Assisted Production of Biodiesel to Reduce Toxicants in Diesel Generator Emissions

Ngee S. Chong ^{1,*}, Ifeanyi Nwobodo ², Madison Strait ³, Dakota Cook ⁴, Saidi Abdulramoni ⁵ and Beng G. Ooi ^{1,*}

- Department of Chemistry, Middle Tennessee State University, Murfreesboro, TN 37132, USA
- Jacam Catalyst, Gardendale, TX 79758, USA; ifeanyi.nwobodo@jacamcatalyst.com
- Department of Chemistry, Iowa State University, Ames, IA 50011, USA; mastrait@iastate.edu
- Department of Food, Nutrition and Culinary Sciences, Clemson University, Clemson, SC 29634, USA; dakotadcook98@gmail.com
- Catalent Pharma Solutions, Bloomington, IN 08873, USA; saidi.abdulramoni@catalent.com
- * Correspondence: ngee.chong@mtsu.edu (N.S.C.); beng.ooi@mtsu.edu (B.G.O.)

Abstract: The environmentally sustainable production of biodiesel is important for providing both a renewable alternative transportation fuel as well as a fuel for power generation using diesel engines. This research evaluates the use of inexpensive catalysts derived from waste materials for converting triglycerides in seed oils into biodiesel composed of fatty acid methyl esters. The performance of CaO catalysts derived from the shells of oysters, mussels, lobsters, and chicken eggs was investigated. The shell-derived powders were calcined with and without the addition of zinc nitrate at 700–1000 °C for 4 h to yield CaO whereas the CaO-ZnO mixed catalyst were prepared by wet impregnation followed by calcination at 700 °C. The catalysts were characterized by XRF, XRD, TGA, SEM, FTIR and GC-MS. The CaO-ZnO catalysts showed slightly better conversion efficiency compared to CaO catalysts for the transesterification of canola oil. The mixed CaO-ZnO catalysts derived mainly from oyster shells showed the highest catalytic activity with >90% biodiesel yield at a 9:1 methanol-to-oil mole ratio within 10 min of ultrasonication. The reduction of toxicant emission from the generator is 43% and 60% for SO₂, 11% and 26% for CO, were observed for the biodiesel blending levels of B20 and B40, respectively.

Keywords: biodiesel production; ultrasonication-assisted synthesis; transesterification catalysts; shell-derived CaO and CaO/ZnO; calcination of oyster, mussel, lobster, and egg shells; B20 and B40 biodiesel emission profiles; CO and SO_2 emission; generator emissions of toxicants



Citation: Chong, N.S.; Nwobodo, I.; Strait, M.; Cook, D.; Abdulramoni, S.; Ooi, B.G. Preparation and Characterization of Shell-Based CaO Catalysts for Ultrasonication-Assisted Production of Biodiesel to Reduce Toxicants in Diesel Generator Emissions. *Energies* **2023**, *16*, 5408. https://doi.org/10.3390/en16145408

Academic Editors: Tae Hyun Kim and A.V.S.L. Sai Bharadwaj

Received: 16 June 2023 Revised: 30 June 2023 Accepted: 5 July 2023 Published: 16 July 2023



Copyright: © 2023 by the authors. Licensee MDPI, Basel, Switzerland. This article is an open access article distributed under the terms and conditions of the Creative Commons Attribution (CC BY) license (https://creativecommons.org/licenses/by/4.0/).

1. Introduction

Biodiesel has become one of the major alternative energy sources to replace fossil fuel, due to its advantages including reduced emissions, low toxicity, and environmental sustainability. Besides, biodiesel is produced from renewable sources such as oilseeds from edible and non-edible crops, animal fat, and microorganisms which makes it a viable fuel from a sustainability viewpoint [1]. The increased interest in biodiesel fuel as an alternative source of energy is due to its beneficial aspects in the reduction of greenhouse gases, improvement in energy security, and as a means of generating revenue [2]. The current global climate change and depletion of natural resources are partly related to the excessive dependence on fossil fuels to meet energy needs. Scientists have anticipated that fossil fuels might run out in 2050 due to the enormous demand and utilization of fossil resources [3]. Petroleum-based fuels are derived from the finite oil reserves in certain regions of the world. Consequently, those countries with limited oil production and refining capacity are confronted with a foreign exchange crisis, basically due to the importation of petroleum products. Therefore, it is imperative to look for alternative fuels that can be produced from renewable materials [4].

Energies 2023, 16, 5408 2 of 20

Biofuels such as bioethanol and biodiesel have been proposed for use in internal combustion engines. Biodiesel could reduce the emission of hydrocarbons and CO by up to 70% and 50%, respectively, compared to petroleum diesel. Furthermore, biofuels can be blended with petroleum-based fuels with little or no engine modification [5]. Biodiesel has higher density and kinematic viscosity values compared to petroleum diesel, which infers that biodiesel has greater energy density output and better lubricity than petroleum diesel. The high cetane number is an indication of the diesel ignition quality and completeness of fuel combustion whereas its high flash point ensures safer storage and handling [6]. Biodiesel is composed of fatty acid alkyl esters obtained by the transesterification of vegetable oil or animal fat [7]. Biodiesel is a non-petroleum-based fuel, or an alternative fuel produced by the transesterification reaction between a vegetable oil or animal fat and methanol or ethanol in the presence of an appropriate catalyst (homogenous, heterogeneous, or enzyme-based catalyst) [8].

Biodiesel is a promising alternative to fossil fuel and is comprised of mono-alkyl esters of long-chain fatty acids derived from renewable feedstocks designated B100. A mono-alkyl ester is the reaction product of straight-chain alcohol like methanol or ethanol, with triglyceride (fat or oil), which also produces glycerin or glycerol. Biodiesel can be used as B100 (neat) or in a blend with petroleum diesel. There are different blends of biodiesel with ultralow sulfur petroleum diesel (ULSPD) ranging from 1% to 50% [9]. A blend of 20% biodiesel with 80% petroleum diesel, by volume, is termed B20 and a blend of 40% biodiesel with 60% petroleum diesel is referred to as B40 [9].

Transesterification

Transesterification refers to the reaction of triglyceride (oil or fat) with an alcohol in the presence of a catalyst to form esters and glycerol [10]. Biodiesel produced via transesterification have comparable properties with diesel fuel. Transesterification is also called alcoholysis, because of the reaction of free fatty acid with alcohol. After the transesterification process, the end products (biodiesel or mixture of alkyl esters and glycerol), are separated into two immiscible layers with biodiesel on the top and glycerol settling at the bottom due to their different densities. Methanol and ethanol are common alcohols used in transesterification. If methanol is used to react with triglyceride, the transesterification process is commonly known as methanolysis. During the methanolysis process, heat is applied to the reaction mixture of oil (80–90%) and methanol (10–20%) and 0.5–1.5% (w/w) catalyst. The most commonly used catalyst is NaOH or KOH but other types of homogeneous catalysts based on strong acids and enzymes have also been reported. Heterogeneous catalysts based on Group IIA oxides such as CaO prepared from eggshells have been studied based on the ease of biodiesel product separation and their reusability [11,12]. Statistical analysis has been used to determine the optimum reaction conditions for biodiesel production yield of 93.16% at a temperature of 60.5 °C, methanol to oil ratio of 6.7:1, and catalyst loading of 0.79% (w/w) [13]. Methanol solubility in oil is limited and hence proper mixing is vital. Biodiesel produced from this process is fatty acid methyl ester (FAME). Methanol is preferred for transesterification because it has higher reactivity and is less expensive than other alcohols. When ethanol is reacted with triglyceride, the transesterification process is referred to as ethanolysis. Biodiesel produced using the ethanolysis process contains fatty acid ethyl ester (FAEE). Biodiesel can be used to substitute petroleum-based diesel in engines with minimal changes to the diesel engine because their characteristics are nearly similar [10]. Although most biodiesel production facilities use mechanical stirring, the ultrasonication process has been shown to dissipate energy more efficiently and can improve the transesterification reaction rate constant by 7-9 times relative to mechanical stirring [14].

As shown in Figure 1, the transesterification reaction or alcoholysis of triglycerides from canola, soya bean, and palm oils in the presence of alcohol and catalyst will lead to the formation of alkyl esters or biodiesel and the glycerol by-product. The first step involves the conversion of triglycerides to diglycerides; in the second step, diglycerides

Energies **2023**, 16, 5408 3 of 20

are converted to monoglycerides, and in the final step, monoglycerides are converted to glycerol. Each of the three sequential steps generates biodiesel esters. This process requires 3 moles of alcohol for 1 mole of triglyceride to produce 1 mole of glycerol and 3 moles of fatty acid alkyl esters or biodiesel [15]. Most commercial production processes use 6 moles of methanol for each mole of triglyceride. This excess methanol ensures that the reaction is favorably driven toward the direction of biodiesel production [16].

Figure 1. Transesterification reaction in biodiesel production.

The two main objectives of this study are to evaluate the suitability of four commonly available shell materials for preparing the CaO catalysts used in biodiesel production and assess the degree of reduction of toxicant emissions for biodiesel-blended fuels for powering diesel generators. Most current research publications are aimed at the study of single shell materials including those of chicken egg [11,12,17], abalone [18], snail [19,20], crab [21], scallop [22], lobster [23], oyster [24,25], and mussel [26]. Due to the varying experimental conditions that influence the biodiesel yields, it is difficult to compare the suitability of shell-derived CaO catalysts unless they are evaluated under the same conditions of catalyst loading, methanol-to-oil ratio, reaction time, temperature, stirring rate, and reaction mode (e.g., conventional heating, microwave, or ultrasonication power). This study evaluated the performance of CaO catalysts prepared from the shells of chicken eggs, mussels, oysters, and lobster under the reaction conditions of 1.00 wt.% loading of shell-derived CaO or 5% Zn/CaO catalysts, and 9:1 mole ratio of methanol to canola oil. Furthermore, the environmental benefits of reducing toxicant emissions from power generators using B20 and B40 fuels were compared to the ULSPD diesel fuel. Since power generators are sometimes used indoors and may not be equipped with pollutant reduction devices such as catalytic converters used in cars and trucks, it is necessary to compare the emission profiles of the fuels for the power generators.

2. Materials and Methods

2.1. Materials and Reagents

The seafood waste of shells from mussels, lobsters, oysters and chicken eggs were obtained from local restaurants. The spectroscopic grade methanol from Burdick and Jackson (Muskegon, MI, USA) was used for the transesterification reaction with the canola oil purchased from the local Kroger grocery store. The zinc nitrate hexahydrate from Thermo Fischer Scientific (Waltham, MA, USA). was used for the preparation of the CaO catalyst with zinc. Deuterated chloroform for NMR determination of biodiesel yield was purchased from Cambridge Isotope Laboratories Incorporated (Andover, MA, USA). The ultra-low sulfur petroleum diesel (ULSPD) used for generator emission testing of B20, B40, and ULSPD was purchased from a Shell gas station (Murfreesboro, TN, USA).

2.2. Preliminary Preparation of Shells

The waste shells (mussel, oyster, lobster, and eggshell) were first washed with water to get rid of dirt, other tough impurities, and organic matter on the surface of the shells were scrapped off and rewashed with deionized water before drying the shells in the oven at $115\,^{\circ}\text{C}$ for $15\,\text{h}$.

Energies 2023, 16, 5408 4 of 20

2.2.1. Preparation of CaO Catalyst via Calcination

The dried shells were pulverized using Corona Mill grinder purchased from Amazon (Seattle, WA, USA). The shell powder was calcined in a KSL-1100MX muffle furnace from MTI Corporation (Richmond, CA, USA) at 800 °C and 1000 °C, respectively, at a heating rate of 10 °C per minute for 4 h. The CaO catalyst obtained was transferred into an airtight container kept in the desiccator to prevent the adsorption of atmospheric moisture.

2.2.2. Preparation of CaO-ZnO Mixed Catalyst

The CaO-ZnO mixed catalyst was prepared by a modified wet impregnation method reported by Kumar and Ali [27]. In this preparation, 10.0 g of CaO obtained from the calcined mussel, oyster, lobster, and eggshell were separately suspended in 18 m Ω high purity deionized water before adding dissolved zinc nitrate to the suspension. The zinc nitrate concentration was varied to obtain Zn²⁺ concentration in CaO ranging from 5% (w/w) to 25% (w/w). The slurry was stirred for 4 h with a magnetic stirrer at room temperature before being dried in the oven at 120 °C for 24 h. The dried mixture was calcined at 700 °C for 4 h in the muffle furnace.

2.3. Catalyst Characterization

A Thermo Scientific™ Niton XL3t Ultra X-ray fluorescence analyzer (Billerica, MA, USA) was used to determine the elemental composition of the uncalcined and calcined shell samples using the Test All Geo Method with a spectral acquisition time of 4 min.

The Rigaku Miniflex 600 X-ray powder diffractometer (Tokyo, Japan) was used to analyze the crystalline phases and diffraction pattern of the shell-derived catalysts and CaO-ZnO mixed catalyst. The Rigaku Miniflex was operated at 40 kV tube voltage and 15 mA tube current using $\text{Cu}(\text{K}\alpha)$ radiation at the speed of $1^\circ/\text{min}$ over a 2θ range from 10° to 70° with a step size of 0.010° .

The Varian 7000 Fourier transform infrared spectrometer (Varian Inc., Walnut Creek, CA, USA) was used to confirm the presence of characteristic absorption bands and to distinguish among the calcium forms of carbonate, oxide, and hydroxide present in the uncalcined shell, calcined shell (CaO) and CaO-ZnO mixed catalyst. FTIR spectral measurements were obtained in the wavenumber range of 400–4000 cm⁻¹ at a resolution of 4 cm⁻¹ with 32 co-added scans and Happ-Genzel apodization using a HgCdTe detector cooled with liquid nitrogen. The concentrations of carbon monoxide, formaldehyde, methane, and ethylene were determined using the Varian FTIR spectrometer with a 10-m pathlength gas cell.

The Hitachi (Schaumburg, IL, USA) S-3400N scanning electron microscope (SEM) was used to determine the morphological characteristics and surface structure of the shell derived catalysts. The elemental composition of samples was analyzed by Oxford Instruments (High Wycombe, UK) energy-dispersive X-ray detector (EDX). The SEM-EDX analysis was carried out with and without the use of the gold-palladium sputter coater to get optimal results with SEM imaging and elemental analysis.

The Q500 thermogravimetric analyzer (TA Instruments, New Castle, DE, USA) was used to characterize the profile of mass loss in uncalcined shell powders as a function of temperature from 20 $^{\circ}$ C to 1000 $^{\circ}$ C. The decomposition patterns of shell samples from chicken eggs, oysters, mussels, and lobsters were determined.

2.4. Ultrasonication-Assisted Biodiesel Synthesis and Yield Measurement

The catalytic efficiency for the transesterification of canola oil and methanol was carried out using the Hielscher model UP200St ultrasonication equipment (Teltow, Germany). The ultrasonic processor is equipped with an ultrasonic transducer, sonotrode, generator, temperature sensor, power supply and other attachments.

The loading of 1% (w/v) catalyst (e.g., mussel-CaO, oyster-CaO, egg-CaO, lobster-CaO, mussel-CaO-ZnO, oyster-CaO-ZnO, egg-CaO-ZnO, lobster-CaO-ZnO) was prepared by mixing 0.25 g of each catalyst with 9.75 mL of methanol and stirred for about 15 min before

Energies **2023**, 16, 5408 5 of 20

adding 25 mL canola oil. The mixture was preheated to 60 °C and the ultrasonication was carried out for 10 min with 9:1 methanol to canola oil mole ratio. The reaction was performed in a 100-mL container with ultrasonication operating conditions of 100% amplitude, 100% pulse, 180 W power, and an operating frequency of 26 kHz. The biodiesel upper layer was separated from the glycerol bottom layer by centrifugation. The percentage conversion of triglyceride into FAME was determined using the JEOL 500 MHz 1 H-NMR (Peabody, MA, USA). The biodiesel yields were calculated by comparing the integrated signals of the methoxy hydrogen and the α -methylene hydrogen as described earlier [28].

2.5. GC-MS Analysis of Diesel Generator Emissions

A Yanmar 4000-watt diesel power generator was used to evaluate the emissions of B20, B40, and ULSPD fuels by directing the generator exhausts through a 5-foot copper tubing of 0.25-inch outer diameter for cooling the diesel engine emissions before collecting the gas samples in 3-L Tedlar bags that were subsequently attached to the Nutech autosampler for GC-MS analysis.

An Agilent 6890 gas chromatograph interfaced with an Agilent 5973 quadrupole mass spectrometer (GC-MS) (Agilent Technologies, Santa Clara, CA, USA) were used for the analysis of emission samples from the generator fueled with biodiesel-blended fuels. A 16-position Nutech autosampler for automated sequential analysis was used to introduce 20.0 mL of gas samples into the Agilent GC-MS via the Nutech 8900DS preconcentrator (GD Environmental Supplies, Inc., Richardson, TX, USA). The preconcentrator has three cryogenic traps including the glass bead trap, Tenax TA trap and the cryofocuser for the selective enrichment of the volatile organic compounds (VOCs) in the samples by controlling the trap temperatures and desorption time settings to achieve low detection limits. The detailed preconcentrator and GC-MS conditions were described in a previous publication [29]. Agilent ChemStation and Markes TargetView V2.0 software were used to process the GC-MS data via the use of the mass spectral database from the National Institute of Standards and Technology.

3. Results

3.1. Catalyst Characterization

3.1.1. Thermogravimetric Analysis (TGA)

TGA was used to measure the change in weight of various shell materials as a function of temperature and hence reveal the decomposition patterns of the shells at the temperature range of 20 °C to 1000 °C. As shown in Figure 2a,b for the mussel and lobster shell samples, the shells are composed mainly of calcium carbonate which decomposes into calcium oxide and carbon dioxide at approximately 800 °C and above. The variation seen in the thermal curve of the oyster, mussel, lobster, and eggshell is due to the different structural compositions of the individual shells. These shells may also contain other forms of carbonates together with CaCO3. Figure 1a shows the decomposition pattern of the mussel shell with the weight loss occurring in two stages. The weight loss between 100 °C–440 °C is due to the organic impurities breaking down in the mussel shell powder. About 3.42% sample weight loss is shown at this temperature range. A significant weight loss was measured at 560 °C–810 °C which is displayed in the derivative weight loss curve of the shell in blue color (Figure 2a). This weight loss measured is due to the CO2 released from the decomposition of CaCO3.

$$CaCO_3$$
 (s) \longrightarrow CaO (s) $+$ CO_2 (g)

The observed weight loss of 41.75% from the mussel shell sample is close to the actual weight percent of CO_2 in $CaCO_3$ at 44%. This indicates that CO_2 was lost during thermal decomposition and the mussel sample was converted to CaO at 810 °C. Above 810 °C, there is no further change in the weight of the mussel shell because the sample has been completely converted to CaO.

Energies 2023, 16, 5408 6 of 20

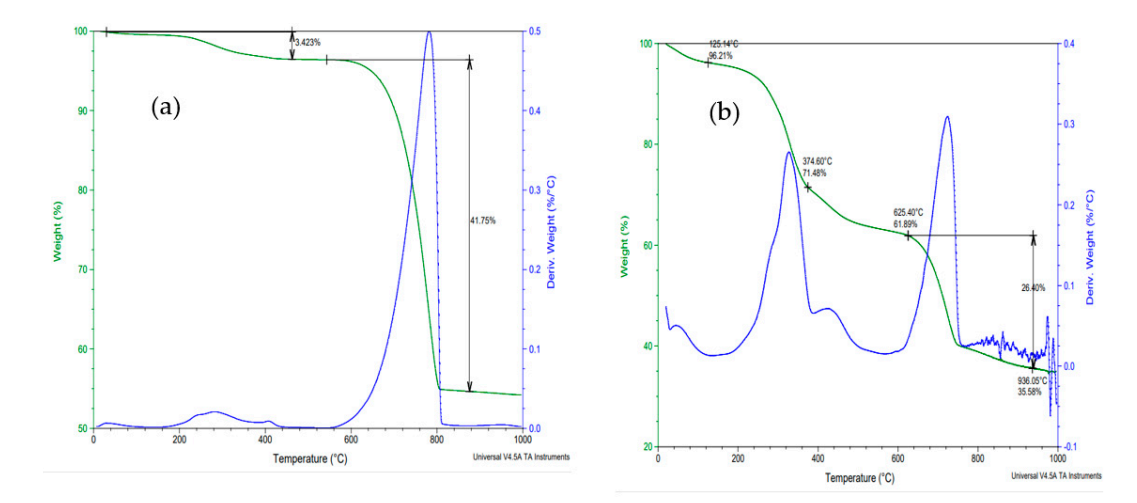


Figure 2. TGA plots for calcination of (a) mussel shell and (b) lobster shell. Note that the Y-axes correspond to the weight % and change in weight % per degree Celsius for the regular TGA plot (green) and first derivative TGA plot (blue), respectively.

The chicken eggshell decomposition pattern also occurred in two stages as shown in Figure 3. The weight loss seen between 200 °C–480 °C is associated with the different organic impurities in the eggshell powder. This accounts for about 6.92% of the sample weight loss. A substantial weight loss of 41.74% can be seen from the thermal curve of the second stage at a temperature range of 600 °C–825 °C due to the $\rm CO_2$ evolved from the decomposed $\rm CaCO_3$. Unlike the mussel and the eggshell, the oyster shell decomposition pattern occurred in a single step. A weight loss of 44.05% from the oyster shell is attributed to the actual weight percent of $\rm CO_2$ lost during the thermal decomposition of calcium carbonate of the shell into calcium oxide. This is an indication that the crystalline structure of the oyster shell is composed almost exclusively of $\rm CaCO_3$ with no organic constituents found in either chicken eggshell or lobster shell. The thermal decomposition curve shows a significant weight loss between the temperature range of 560 °C–785 °C. At a temperature of 785 °C and above, the oyster shell is completely converted to $\rm CaO_3$ and the sample weight remained constant at this point.

The lobster shell decomposition pattern occurred in three distinct stages. From Figure 2b shown above, it could be seen that the decomposition of the lobster shell started very early at a lower temperature range between $20-125\,^{\circ}\text{C}$ due to the loss of water (3.79%) present in its structure. Unlike oyster shell which is composed mainly of CaCO₃, the lobster shell contains water, proteins and chitins which account for 38.11% of the weight loss at the temperature range of $20-625\,^{\circ}\text{C}$. This was followed by the gradual decomposition of its CaCO₃ after 625 $^{\circ}\text{C}$ to CaO with loss of CO₂. Romano et al. 2007 reported similar findings for TGA of lobster cuticles that chitin degradation occurred between 270 $^{\circ}\text{C}$ to about 600 $^{\circ}\text{C}$ followed by decarboxylation of CaCO₃ after 650 $^{\circ}\text{C}$ [30].

The major component of the four types of shells is calcium carbonate which decomposes into calcium oxide and carbon dioxide. The weight loss of about 44% in the shell sample is attributed to the actual weight percent of CO_2 (in $CaCO_3$), released during the decomposition process. There is a variation in temperature at which each of these shell samples attain complete conversion into CaO. A temperature of $800\,^{\circ}C$ and above is required for the complete conversion of mussel, egg, and lobster shells into CaO whereas at a temperature below $800\,^{\circ}C$, around $785\,^{\circ}C$, the oyster shell is completely converted into CaO. This is due to the different structural compositions of the shells and the varying levels of organic impurities present in some of the shell samples.

Energies **2023**, 16, 5408 7 of 20

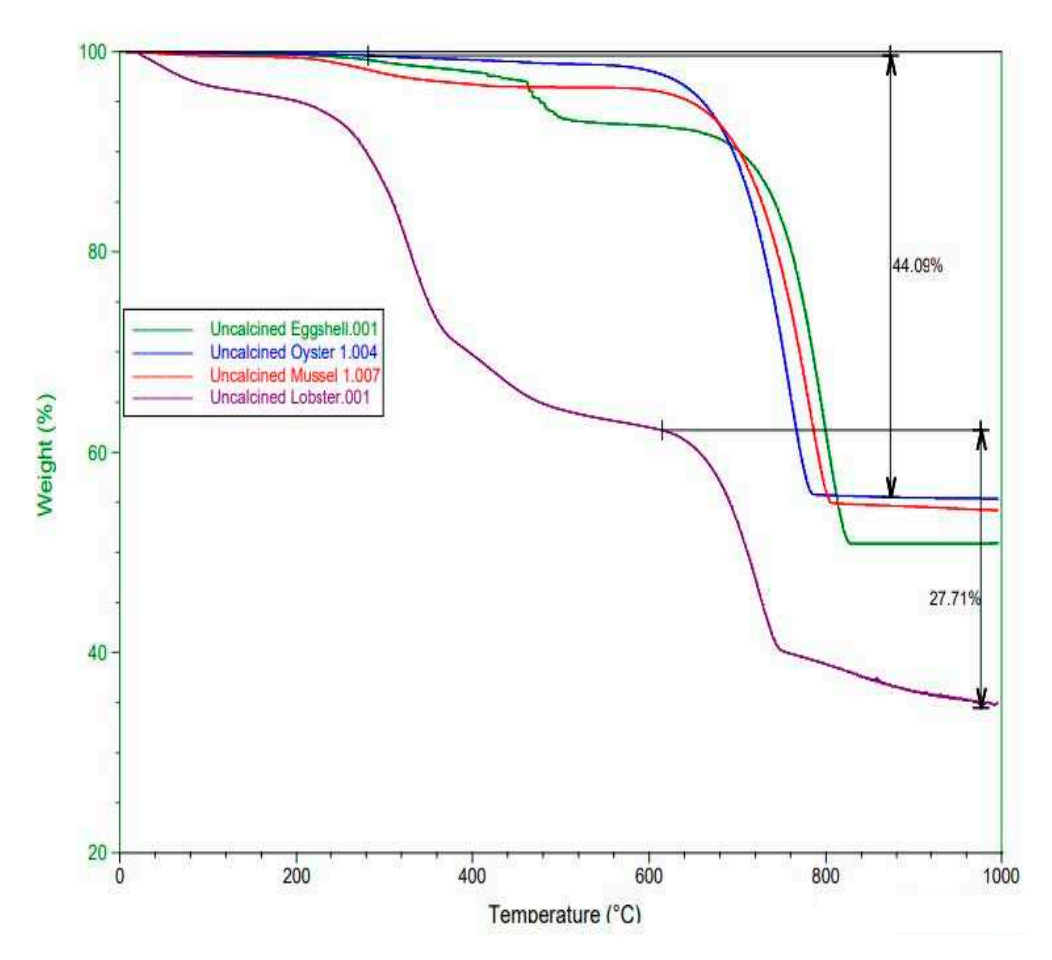


Figure 3. Comparative TGA plots for calcination of shell-derived powders from chicken egg (green), oyster (blue), mussel (red), and lobster (purple).

3.1.2. Characterization of Catalysts by SEM/EDX and XRF Methods

The shell-derived CaO catalysts prepared from four different sources of seafood or chicken egg wastes were characterized by SEM/EDX and the SEM images are shown in Figure 4. The comparison of calcined oyster shell and lobster shell are shown in Figure 4a,b, respectively, at the same magnification of 1000-fold with the micron scale bar shown. The oyster-derived CaO particles are larger and more crystalline than the particles of lobster shell which are composed of 7.8% phosphate in addition to 92.2% carbonate as the primary anions. There is also a direct correlation between calcium and phosphorus levels for lobster shells from different body parts including cephalon, thorax, abdomen, uropod, legs, and chela [31]. The EDX elemental data shows that the calcined lobster shell contains 3.2% magnesium, 0.34% strontium, and 0.28% sodium in comparison to the calcined oyster shell crystallites which show only 0.2% magnesium. The chicken eggshell sample shows the smallest particle size. The calcination of the shell samples at 1000 °C changed the composition and the structure of the shell with a resultant increase in the surface area and better catalytic activity. After calcination, some particles show the features of holes (Figure 4c) associated with the loss of CO₂ or collapse of the mesoporous structure during the initial transformation of CaCO₃ to CaO. The sintering process at 1000 °C allows the aggregation of nanoparticles to form faceted crystallites along with the reduction in surface area and porosity [32].

Energies **2023**, 16, 5408 8 of 20

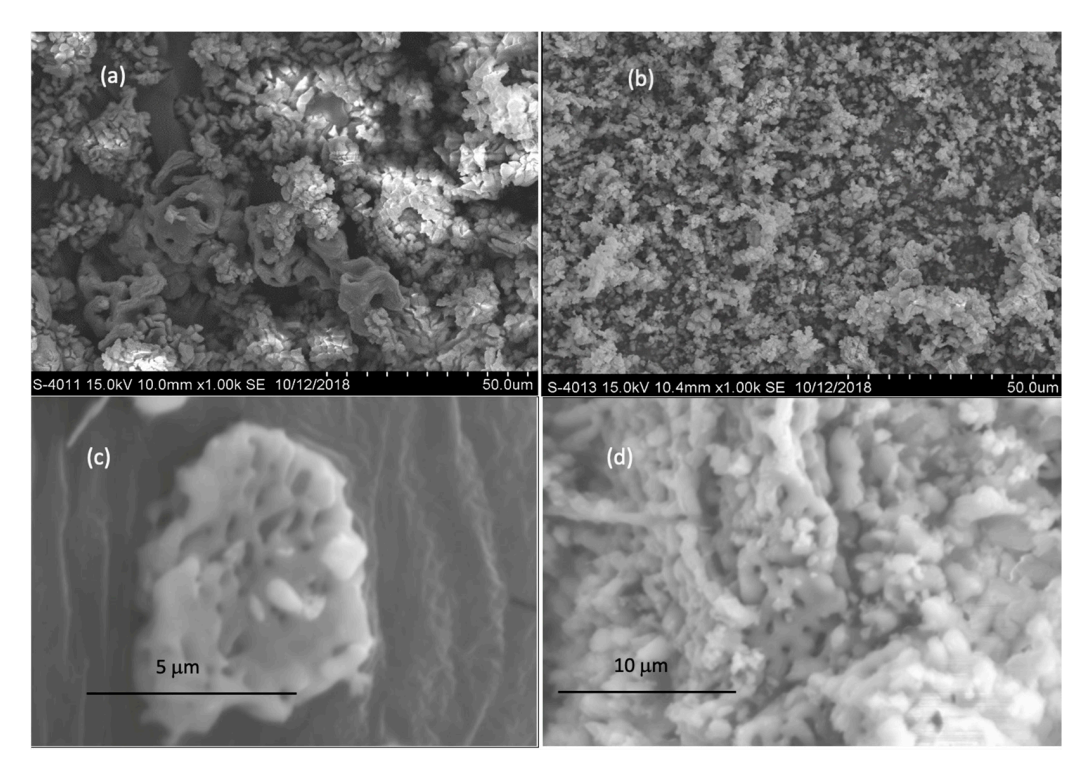


Figure 4. SEM images of (**a**) a calcined sample of oyster shell, (**b**) a calcined sample of lobster shell, (**c**) a calcined sample of mussel shell with 0.29% Zn, and (**d**) a calcined sample of lobster shell with 0.35% Zn.

The calcined lobster shell powders in Figure 4d show the presence of long fibrils of chitin with high carbon content interspersed with CaO particles. The EDX data of calcined shell materials show that the calcium content is the lowest in the lobster samples at 40.4% by weight compared to 45–50 wt.% for the samples of oyster, mussel, and chicken egg. This is due to the presence of other elements including phosphorus, magnesium, and strontium that are either absent or found at lower levels in the other types of shell samples. Phosphorus and magnesium were measured at 1.08 wt.% and 1.86 wt.%, respectively, which are consistent with previously reported values of 0.52–2.41 wt.% phosphorus and 0.33-1.46 wt.% magnesium for various parts of the lobster shell [31]. The 1.08 wt.% phosphorus as phosphate and the 6.95 wt.% carbon in the form of carbonate and organic carbon residue of chitin possess minimal catalytic activity compared to CaO. The Ca:C elemental ratio expressed in atomic or mole percent is also a useful parameter for estimating the degree of calcination, i.e., the higher Ca:O mole ratio of 4.27 for calcined mussel shell and 3.09 for calcined oyster shell implies that they have higher conversion efficiency for forming CaO relative to calcined lobster shell and eggshell. The organic matter in the lobster exoskeleton, mostly chitin, accounts for the 19.7–38.2 wt.% range [33]

The uncalcined and calcined shell powders were also analyzed by XRF and their results were shown in Figure 5. The sums of the seven elements plotted for the four types of shells are given as "SM" values and decreases in the order of mussel (0.86%), lobster (0.57%), oyster (0.37%), and chicken egg (0.14%). The calcium contents of calcined samples [Ca]_c measured in the range of 69.78% to 71.99% agree with the theoretical value of pure CaO at 71.43%. However, the uncalcined samples give XRF values of [Ca]_{uc} in the range of 31.57% to 48.98% following the trend of oyster > mussel, chicken egg > lobster. Uncalcined lobster shell shows the lowest [Ca]_{uc} value of 31.57% and hence gives the smallest yield of CaO for the transesterification reaction.

Energies 2023, 16, 5408 9 of 20

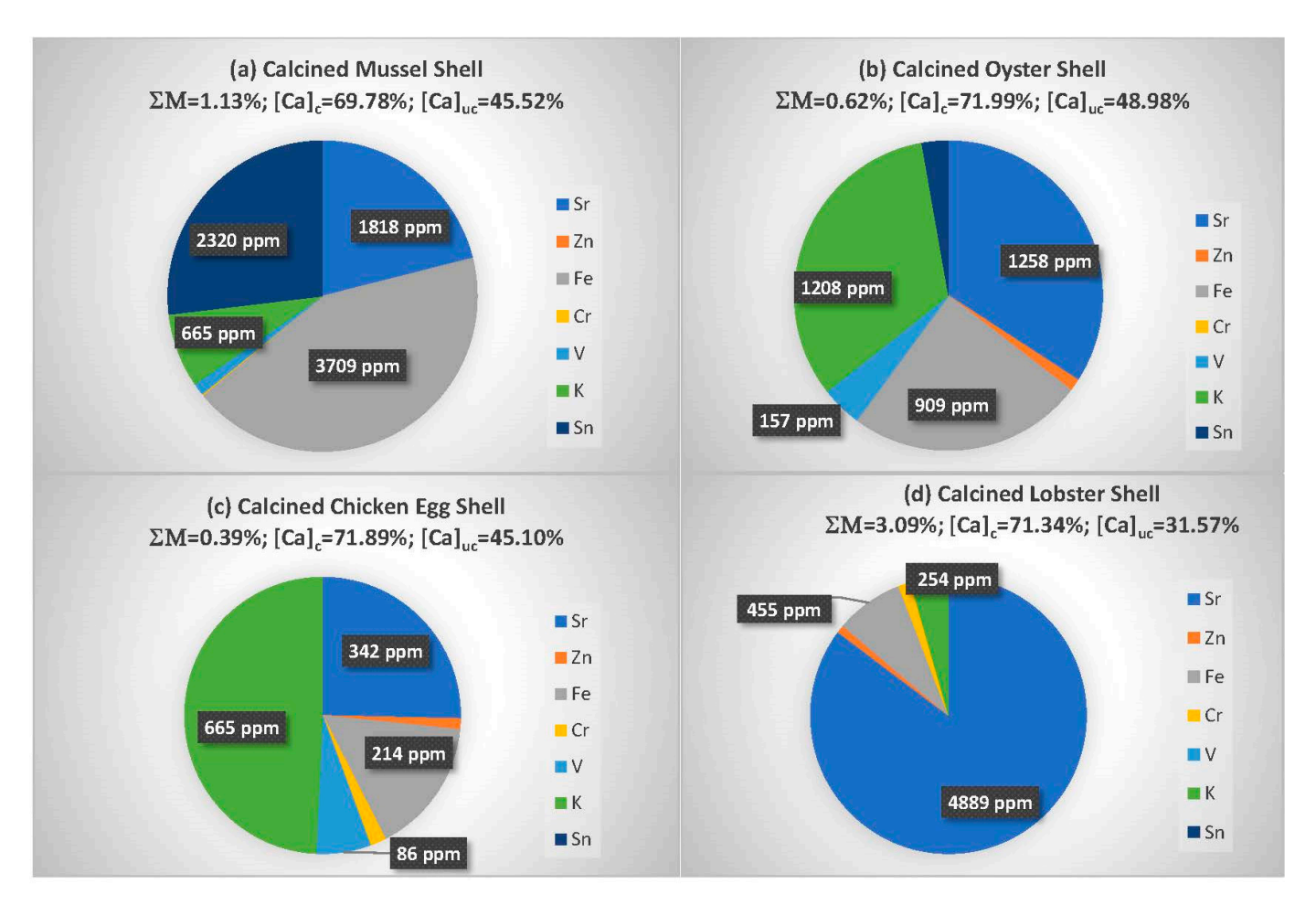


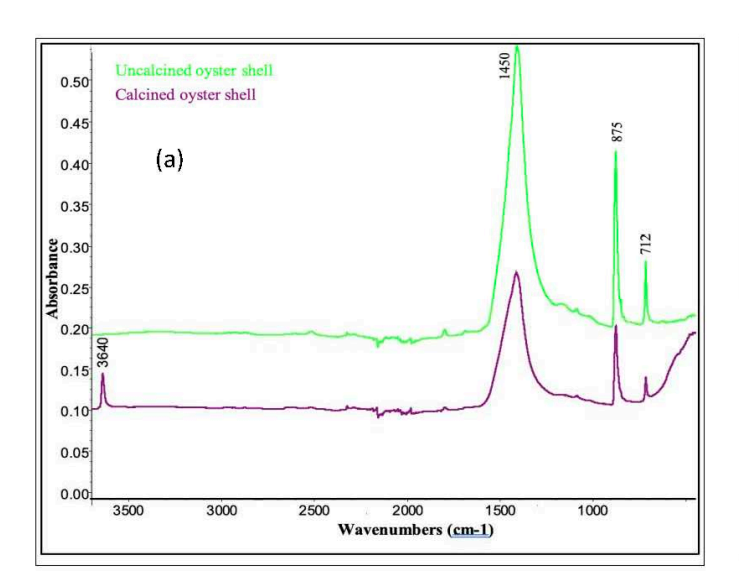
Figure 5. Elemental composition of calcined shell samples of (a) mussel (b) oyster (c) chicken egg, and (d) lobster. The notations of ΣM , $[Ca]_c$, and $[Ca]_{uc}$ stand for sum of metals excluding calcium in percent, percent of calcined calcium, and percent of uncalcined calcium, respectively.

Potassium (1208 \pm 2 ppm) and strontium (1257.6 \pm 0.6 ppm) in the form of oxides for oyster shells are important constituents that can also exhibit strong basicity for producing biodiesel esters. The values of tin at 2320 \pm 0.4 ppm and iron at 3709 \pm 1.4 ppm are observed for calcined mussel shell. Besides calcium, potassium (665 \pm 3.1 ppm) and strontium (4888 \pm 0.6 ppm) are the most abundant trace elements for chicken eggshell and lobster shell, respectively. Among the trace elements measured by XRF, strontium and potassium are potentially important due to the increase in the basicity of K₂O and SrO relative to CaO that may contribute to enhanced reactivity for biodiesel production. The concentrations of strontium are 342 ppm, 1258 ppm, 1818 ppm, and 4889 ppm in calcined shells of chicken egg, oyster, mussel, and lobster, respectively. The values of potassium concentration for calcined shells are 254 ppm for lobster shells, 665 ppm for both mussel and chicken eggshells, and 1208 ppm for oyster shells. The substitution of Ca²⁺ by Sr²⁺ in the crystalline lattice is likely because the cation radius of strontium (Sr^{2+}) is 132 pm compared to 114 pm for calcium (Ca²⁺) whereas Mg²⁺ and K⁺ have significantly different ionic radii of 86 pm and 152 pm, respectively. In general, lattice substitution for ions of the same charge but with a difference in ion radii of less than 15% is highly probable and the ionic radii difference of 15–30% will be less probable [34]. Additional XRF data for the elemental composition of uncalcined and calcined shells are given in Table S1 in the Supplementary Materials.

Energies **2023**, *16*, 5408 10 of 20

3.1.3. FTIR Analysis of CaO and CaO-ZnO Mixed Catalysts Derived from Shell Samples

Figure 6a,b shows the overlaid IR spectrum of the uncalcined and calcined oyster shell, the fundamental absorption bands of $712~\rm cm^{-1}$, $875~\rm cm^{-1}$, and $1450~\rm cm^{-1}$ are indications of asymmetric stretch, out-of-plane bend, and in-plane vibration of C-O bonds of CaCO₃, respectively. There is a noticeable reduction in the intensity of these absorption bands for the calcined shells due to the calcination at high temperatures resulting in the decomposition of the CaCO₃ into CaO and CO₂. The sharp peak at 3640 cm⁻¹ is attributed to OH group stretching in Ca(OH)₂, which is formed upon the exposure of CaO to atmospheric moisture [35]. Similar spectral signals were observed for the mussel shell powder with absorption bands of $716~\rm cm^{-1}$, $863~\rm cm^{-1}$, and $1458~\rm cm^{-1}$ attributed to the asymmetric stretching, out-of-plane bending, and in-plane vibration of the O-C-O bond of CaCO₃. The Ca(OH)₂ peak due to moisture absorption of CaO appears at $3647~\rm cm^{-1}$.



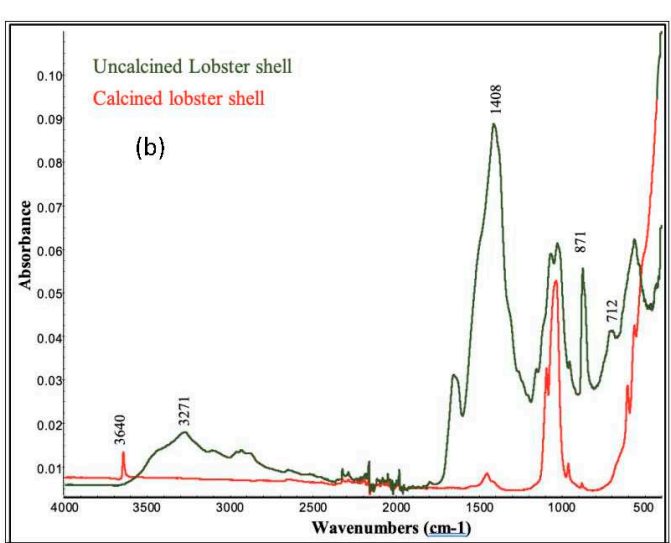


Figure 6. Infrared spectra of uncalcined and calcined samples of (**a**) oyster shell; the absorption bands of 712 cm⁻¹, 875 cm⁻¹, 1450 cm⁻¹ are related to the C-O bonds of CaCO₃. The peak at 3640 cm⁻¹ is due to the O-H stretching in Ca(OH)₂ and (**b**) lobster shell; the absorption bands at 712 cm⁻¹, 871 cm⁻¹ and 1408 cm⁻¹ are related to the C-O bonds of CaCO₃. The peak at 3640 cm⁻¹ is due to the O-H stretching in Ca(OH)₂. The intense peak around 1100 cm⁻¹ is due to the phosphate group in hydroxyapatite [36] whereas the peak at 3271 cm⁻¹ is due to the chitin OH group [37].

The chicken eggshell has characteristic CO_3^{2-} absorption bands at 710 cm⁻¹, 872 cm⁻¹, and 1410 cm⁻¹. The peak at 3644 cm⁻¹ is associated with OH⁻ stretching of Ca(OH)₂ formed from the absorption of moisture by the eggshell-derived CaO. For the lobster shell, the absorption peak indicative of the asymmetric stretch of the C-O bond of CaCO₃ could be seen at 746 cm^{-1} , 872 cm^{-1} , and 1413 cm^{-1} . The sharp peak at 3640 cm^{-1} is attributed to the OH-stretching of Ca(OH)2, which was formed when CaO absorbs atmospheric moisture. The broad peak at $3271 \, \mathrm{cm}^{-1}$ is due to the presence of an OH group of chitin in the lobster shell. The calcination of the shell lead to a decrease in the absorption bands at 1408 cm⁻¹, 871 cm⁻¹ and 712 cm⁻¹ which are associated with CaCO₃. Due to the analytical sampling depth of the attenuated total reflectance accessory for the FTIR spectrometer at about 0.5–2.0 microns, the ratio of the 3640 cm⁻¹ to 1450 cm⁻¹ peaks gives the estimate of the size of the particles with a surface layer of CaO and the underlying CaCO₃ substrate. The heat treatment of shell powders at 5–10 g quantities in the furnace resulted in calcined catalysts with only partial conversion to CaO compared to the complete conversion of 1-2 mg of shell powders in TGA analysis. In reusing the calcined catalysts after multiple batches of catalytic cycles, it is important to monitor the 3640 cm⁻¹ peak and the biodiesel yield to determine when the activity of the catalyst needs to be regenerated via calcination. Energies 2023, 16, 5408 11 of 20

3.1.4. X-ray Diffraction Patterns of the Shell-Derived CaO and CaO-ZnO Mixed Catalysts

The diffractograms obtained from the uncalcined shells in general showed the predominance of CaCO₃ in shell composition. After calcination at 800 °C and 1000 °C, the CaCO₃ originally present in the shells were converted to CaO which could be seen in the diffraction patterns of the calcined shells of mussels and oyster in Figure 6a,b. However, the calcination of lobster shell and chicken eggshell to form CaO is not complete at 800 °C as seen in Figure 6a. The calcined shells showed diffraction peaks characteristic of pure CaO at 20 values of 32.0°, 37.7°, 53.7°, 64.0° and 67.2°; these peaks correspond to the cubic crystal structure associated with the reflections from (111), (200), (220), (311) and (222) planes, respectively [38,39]. For the calcined shell materials produced at 1000 °C for 4 h, the following sets of diffraction peaks with a slight variation of 20 values corresponding to (111), (200), (220), (311) and (222) planes, respectively, were identified as follows:

- Lobster CaO: \rightarrow 32.1°, 37.0°, 53.5°, 63.8° and 67.0°
- Eggshell CaO: \rightarrow 32.3°, 37.5°, 54.0°, 64.5° and 67.5°
- Mussel CaO: \rightarrow 32.8°, 38.0°, 54.5°, 64.8° and 68.1°
- Oyster CaO: \rightarrow 32.8°, 38.0°, 54.5°, 64.8° and 68.1°

These XRD results are similar to those reported by Samantaray et al. [38]. After calcination at 1000 °C for 4 h, all the shell samples were able to attain a similar degree of crystallinity to that of pure CaO. The slightly larger 20 values of mussel CaO and oyster CaO compared to CaO obtained from chicken eggs are likely due to the higher levels of strontium and iron substitution of calcium in the crystalline structures. In Figure 7a, the calcination conditions of 800 °C for 4 h yield XRD diffraction patterns obtained for lobster and eggshell still show the presence of CaCO₃ and other organic constituents besides CaO. For lobster shell that was subjected to heat treatment at 800 °C, the XRD pattern reveals the presence of CaO, MgO and hydroxyapatite that are consistent with the results of previous studies [33,40]. The chitin XRD peaks at 20 values of 9.4, 13.6, 19.7, 21.2, 23.9, 26.8, 28.6, 39.7, 43.0, 78.0 degrees are not observed since chitin would have been degraded after 600/625 °C based on TGA plots shown in Figure 2b and published results of Romano et al. [30,37]. Purer shell materials without phosphate-based constituents like hydroxyapatite will show the decomposition of CaCO₃ into CaO at calcination temperatures of 800 °C [41]. The TGA analyses of the shell samples confirmed that the lobster and eggshell contain more organic impurities in their structures thereby requiring a higher calcination temperature above 800 °C, preferably 1000 °C, to attain the crystalline phase of CaO.

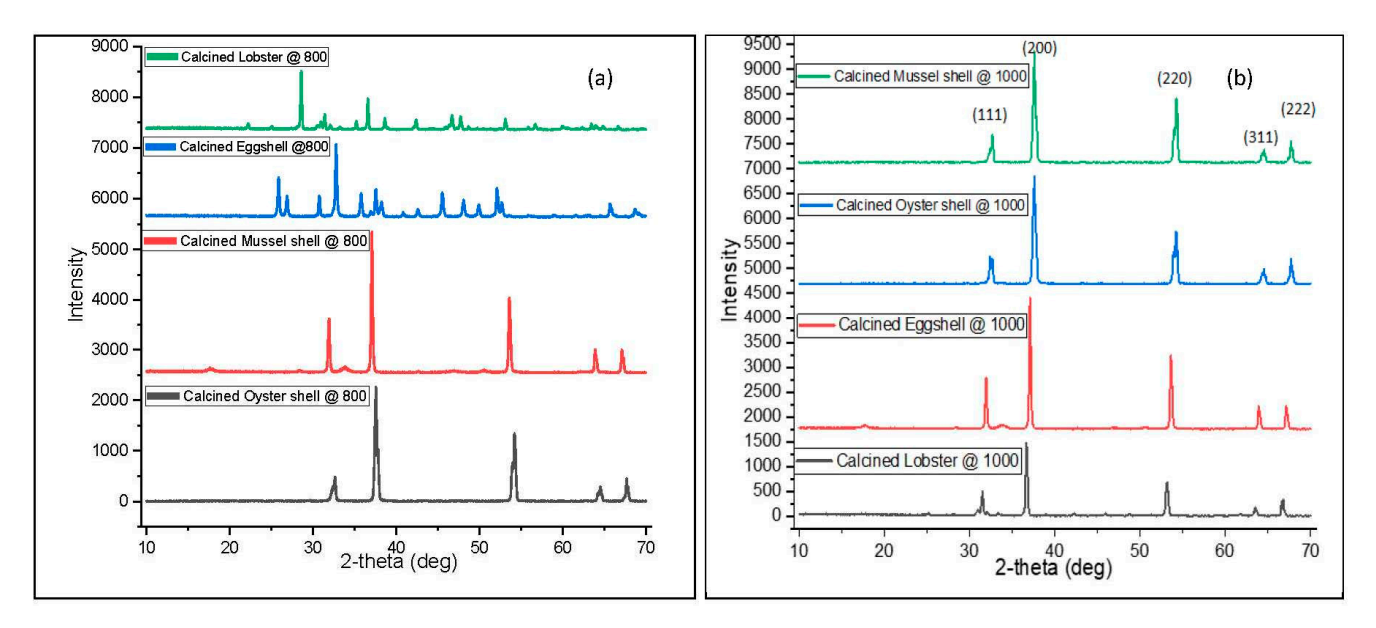


Figure 7. Powder X-ray diffraction patterns of CaO catalysts derived from various shell materials calcined at **(a)** 800 °C and **(b)** 1000 °C.

Energies 2023, 16, 5408 12 of 20

Figure 8a compares XRD patterns of CaO-ZnO mixed metal oxide catalysts prepared with 5 wt.% zinc concentration at 700 °C calcination temperature. The XRD diffraction patterns of 5% Zn-oyster-CaO, 5% Zn-mussel-CaO, 5% Zn-lobster-CaO and 5% Zn-eggshell-CaO show the exclusive presence of CaO in cubic crystalline phase in all the calcined materials except the 5% Zn-lobster-CaO material that shows tiny XRD peaks belonging to hydroxyapatite in addition to the Zn. When the Zn levels were studied at 5%, 7%, 10%, and 25% wt.% in the calcined oyster samples, the distinct peaks corresponding to the ZnO phase were only observed when calcined samples with Zn²⁺ concentrations of 10 wt.%, 25 wt.%, and the reference ZnO samples were prepared from Zn nitrate at 700 $^{\circ}$ C as shown in Figure 8b. Nevertheless, a further increase in the Zn^{2+} concentration (≥ 7 wt.%) in the shell-derived CaO leads to formation of ZnO in the hexagonal phase which is seen in the low-intensity peaks at 2θ (10% Zn-oyster-CaO) = 34.45° , 56.62° , and 62.89° and 2θ (25% Zn-oyster-CaO) = 34.0° , 56.18° , and 62.18° . This result is similar to the work reported by Kumar and Ali [27]. The diffraction peak obtained for Zn nitrate calcined at the same temperature of 700 °C for 4 h matches some of the characteristic peaks of ZnO at 20 (Calcined Zn(NO₃)₂ at 700 °C) = 34.04°, 47.22°, 56.37° and 62.7°. The increase of Zn²⁺ concentration from 5 wt.% to above 7 wt.% (i.e., 10 wt.% and 25 wt.%) leads to the formation of two distinct phases of CaO-ZnO. The American Mineralogist Crystallography Database information for the XRD patterns of oxides in the calcined materials is provided in the Table S2 of the Supplementary Materials.

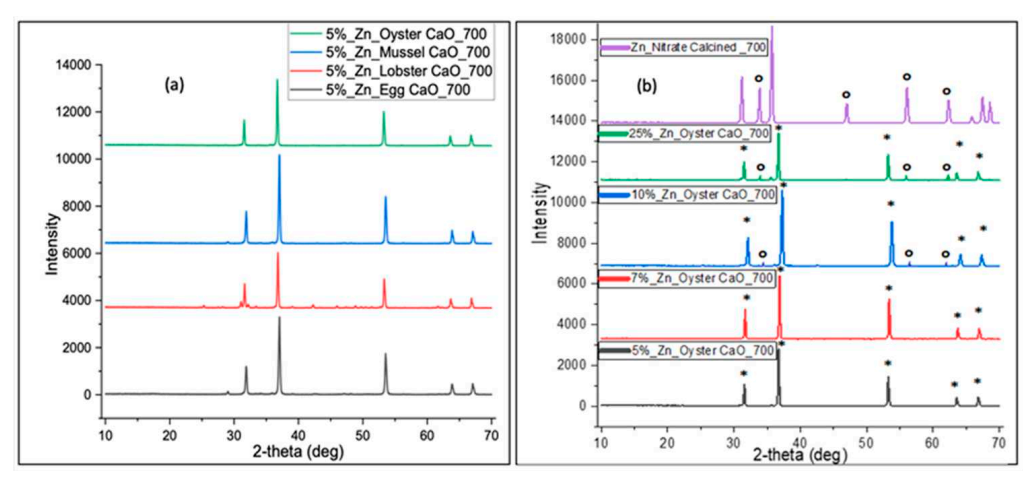


Figure 8. (a) XRD patterns of 5% Zn-Oyster-CaO, 5% Zn-Mussel-CaO, 5% Zn-Eggshell-CaO and 5% Zn-Lobster-CaO calcined at 700 °C for 4 h. (b) XRD patterns of 5% Zn-Oyster-CaO, 7% Zn-Oyster-CaO, 10% Zn-Oyster-CaO, 25% Zn-Oyster-CaO, and $Zn(NO_3)_2$ calcined at 700 °C for 4 h (*: CaO phase; o: ZnO phase).

3.2. Comparison of Biodiesel Yields Using Different Calcined Catalysts

The experimental biodiesel yields for various catalysts are summarized in Table 1. The calculation of yields is based on the NMR measurements of the ratios of the a-methylene protons to methoxy protons in reaction products as explained in a prior study [28]. The catalytic activity of the individual shell-derived CaO including oyster CaO, mussel CaO, lobster CaO and eggshell CaO have been investigated and compared to the activities of Zn-spiked CaO mixed metal oxide catalysts of 5% Zn-oyster-CaO, 5% Zn-mussel-CaO, 5% Zn-lobster-CaO, 5% Zn-eggshell-CaO. The ultrasonication-assisted transesterification reaction conditions are 1 wt.% catalyst loading, 9:1 methanol to oil mole ratio, reaction temperature of 60 °C and ultrasonication time of 10 min. The percentage conversion of triglycerides in the canola oil into biodiesel by CaO catalysts derived from the shells of oysters, mussels, chicken eggs, and lobsters were 92.9%, 89.0%, 90.3% and 50.6%, respectively. The oyster-derived CaO catalyst showed the best biodiesel yield due to the highest level of calcium content in the chemical composition of both uncalcined and calcined materials as revealed by XRF analysis, crystallite size and morphology that provide a large surface area for

Energies **2023**, 16, 5408 13 of 20

transesterification, and concentrations of trace transition metals in the crystalline structure to augment the catalyst activity of the shell-derived CaO. There is not much loss of yield when using waste-shell-based CaO in comparison to pure CaO [42].

The spiking of the shell-derived CaO with Zn²⁺ (i.e., 5 wt.% Zn²⁺ concentration in CaO), resulted in increased biodiesel yields of fatty acid methyl esters (FAME) for all the shell-based catalysts used in this study. As shown in Table 1, the CaO-ZnO mixed metal oxide catalysts showed higher biodiesel yields than the CaO counterparts under the same reaction conditions. The 5% Zn-oyster-CaO, 5% Zn-mussel-CaO, 5% Zn-eggshell-CaO, and 5% Zn-lobster-CaO recorded biodiesel percentage yields of 93.9%, 92.8%, 92.5% and 59.5%, respectively. The highest observed FAME yield for oyster-CaO-ZnO (with 5% of Zn²⁺ concentration) can be related to its basic properties, as biodiesel yield increases with the increasing number of basic sites [27,43]. Kumar and Ali reported that the catalytic activity of the ZnO-CaO catalyst toward the transesterification reaction of biodiesel production was found to be a function of their basic strength and in the case of Zn/CaO weight ratio, the maximum basic strength was observed for CaO-ZnO at 1.5–7% Zn²⁺ concentration [27]. The EDX measurements of zinc showed that the actual Zn levels in the Zn/CaO mixed catalyst were only 1.78–3.41 wt.% instead of the targeted 5 wt.% Zn-spiked CaO catalyst. Further increase in Zn²⁺ levels in the CaO-ZnO mixed metal oxide catalyst beyond 1.5% resulted in a decrease in biodiesel yield as can be seen in the comparative study of Zn²⁺ concentrations in 5% Zn-oyster-CaO, 7% Zn-oyster-CaO, and 10% Zn-oyster-CaO mixed catalyst, which produced biodiesel yields of 93.9%, 67.2%, and 62.3%, respectively.

It is inconclusive from the results of Table 1 that the biodiesel yields in this study are improved by the preparation of mixed oxide catalysts that contain ZnO. Although there are slight increases of 1.0% for oyster-based catalysts and 2.3% for catalysts prepared from chicken eggshells, they are smaller than the pooled standard deviation of 2.35%. In the case of mussel-based catalysts, there is a decrease in the biodiesel yield of 3.8%. For comparison in the case of lobster, there is a statistically significant increase in its yield of 9.9% when a mixed oxide catalyst containing ZnO was used. In a study conducted using CaO prepared from snail shells, the waste palm cooking oil showed a biodiesel yield of 80% for CaO and 90% for CaO modified with ZnO [20]. A remarkable aspect of the present study is the reaction time of 10 min for ultrasonication-assisted reaction compared to 45–360 min for the cited studies describing biodiesel synthesis using a hotplate.

Table 1. Comparison of biodiesel yields for different CaO catalysts and reaction conditions. The current study is based on the use of 1.00 wt.% shell-derived CaO or 5% Zn/CaO catalysts, and 9:1 mole ratio of methanol to canola oil.

Catalyst (Weight %)	Method	Time (min)	Yield (%)
Oyster CaO (1%)	Present ultrasonication study	10	92.9
Mussel CaO (1%)	Present ultrasonication study	10	89.0
Eggshell CaO (1%)	Present ultrasonication study	10	90.3
Lobster CaO (1%)	Present ultrasonication study	10	50.6
5%Zn-Mussel-CaO (1%)	Present ultrasonication study	10	92.8
5%Zn-Eggshell-CaO (1%)	Present ultrasonication study	10	92.5
5%Zn-Lobster-CaO (1%)	Present ultrasonication study	10	59.5
5%Zn-Oyster-CaO (1%)	Present ultrasonication study	10	93.9
7%Zn-Oyster-CaO (1%)	Present ultrasonication study	10	67.2
10%Zn-Oyster-CaO (1%)	Present ultrasonication study	10	62.3
CaO (3%)	Hotplate with stirring, 25:1 CH ₃ OH-jatropha oil, [44]	180	91

Energies **2023**, *16*, 5408 14 of 20

Table 1. Cont.

Catalyst (Weight %)	Method	Time (min)	Yield (%)
CaO-ZnO (3%)	Hotplate with stirring, 25:1 CH_3OH -jatropha oil, [44]	180	94
CaZn ₂ (OH) ₆ .2H ₂ O (2%)	Hotplate with stirring, 10:1 CH ₃ OH-sunflower oil, [45]	120	92
1.5-Zn/CaO-550 (5%)	Hotplate with stirring, 9:1 CH ₃ OH-cottonseed oil, 1.5 wt.% Zn-CaO calcined at 550 °C [27]	45	>99
CaO-ZnO (10%)	Hotplate with stirring, 40:1 CH ₃ OH-soybean oil, [46]	360	73
Eggshell CaO (6.04%)	Ultrasonication 299.7 W; 8.3:1 CH ₃ OH-waste cooking oil, 55 °C [12]	39.8	98.6
Crab shell CaO (3%)	250 rpm stirring rate; 9:1 CH ₃ OH-fishmeal plant oil, 60 $^{\circ}$ C [21]	60	88.2
Snail shell CaO (3%)	Heating mantle, 65 °C; 6:1 CH ₃ OH-waste palm cooking oil [20]	180	80

3.3. Emissions of Biodiesel Fuel Blends in Diesel Generators

Diesel generators are commonly used in countries where electric power grid infrastructures are very minimal or sparse in rural areas or even cities due to budgetary constraints. Diesel generators are easy to install and are frequently used in developing countries in agricultural, residential, and industrial sectors. In Nigeria, the public electricity grid only meets at most 30% of consumer power usage, and most homes have access to public electricity supply for only 6 h daily [47]. The shortfalls in electricity supply account for the installation of 15 million diesel-powered generators in over 90% of businesses and 30% of homes in Nigeria. Due to concerns about the toxicity of carbon monoxide released, inhalable exhaust particulate matter, carcinogens including formaldehyde, 1,3-butadiene, and benzene, and the potential fire risks of diesel fuel, it is important to evaluate the safety of biodiesel fuel blends for use in diesel generators. The California Air Resources Board has developed screening risk assessment tables for diesel engine owners to estimate their overall exposure risk from diesel engine exhaust particulate matter [48]. Since diesel generators are frequently used indoors among businesses and homes, toxicant concentrations will be increased due to the lack of ventilation.

3.3.1. FTIR Analysis of Emissions from Diesel Power Generators

FTIR spectroscopy was used to analyze the small molecular weight compounds in the emissions from diesel power generators. Figure 9 shows the concentrations of carbon monoxide (CO), ethylene (C_2H_4), methane (CH₄), formaldehyde (H_2CO), and sulfur dioxide (SO₂) as the oxygen content of the fuel blends is increased by the fatty acid methyl esters in 20% (B20) and 40% (B40) biodiesel blended with ultralow sulfur petroleum diesel (ULSPD). The 100% ULSPD has significantly higher levels of CO, C_2H_4 , CH₄, H₂CO, and SO₂ relative to the B20 and B40. The emission of highly toxic CO was reduced from 258 ppm in ULSPD emission to 229 ppm and 192 ppm in B20 and B40 emissions, respectively, in the infrared spectral region of 2134–2138 cm⁻¹. The corresponding relative standard deviation is 16.9%, 11.5%, and 3.5% for the CO levels in ULSPD, B20, and B40. The FTIR signals for formaldehyde are in the spectral region of 2683–2949 cm⁻¹. The formaldehyde concentrations of B20 and B40 were reduced by 58% and 59%, respectively, relative to ULSPD. At above 50 ppm, formaldehyde can cause severe pulmonary reactions including pulmonary edema, pneumonia, and bronchial irritation which can result in death. Methane, which is much less toxic than CO and formaldehyde, was measured in the spectral region of

Energies **2023**, *16*, 5408 15 of 20

2874–3188 cm $^{-1}$. The methane concentrations of B20 and B40 were reduced by 39% and 54%, relative to the ULSPD emission.

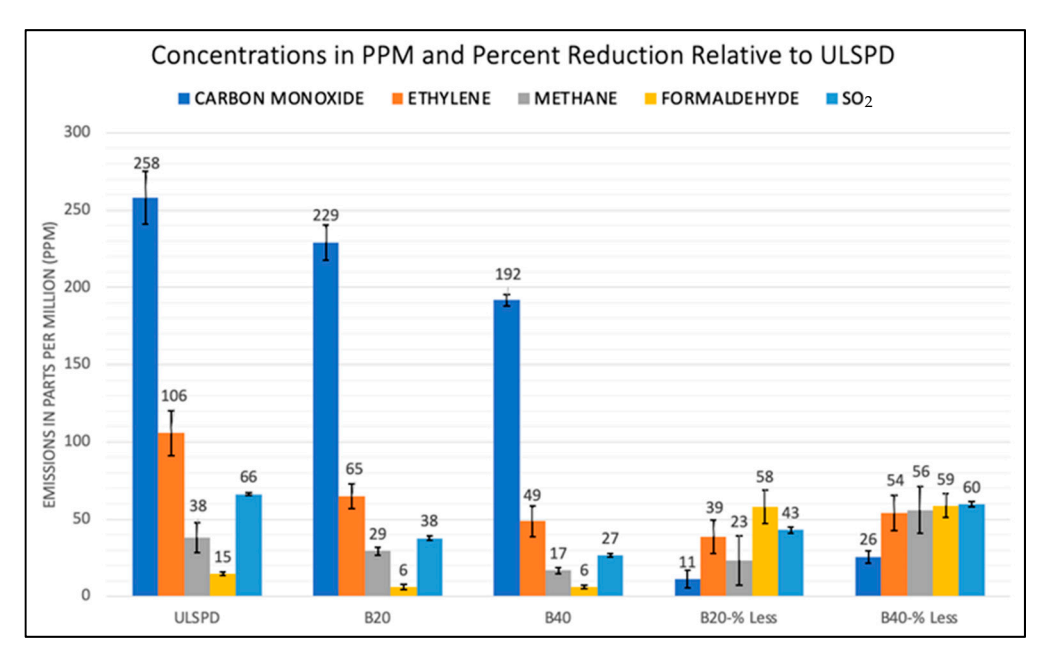


Figure 9. Generator emissions of air pollutants measured by infrared spectroscopy in parts per million units and their percent reduction in B20 and B40 biodiesel fuels relative to ultralow sulfur petroleum diesel (ULSPD).

Due to the adverse human health effects associated with inhalation exposure to diesel emissions, CO is regulated by both the United States Environmental Protection Agency (USEPA) and the Occupational Safety and Health Administration (OSHA). The National Ambient Air Quality Standards of USEPA for CO is 9 ppm for a 24-h period and 35 ppm standard for a 1-h period. The OSHA permissible exposure limit (PEL) for CO is 50 ppm for worker exposure during an 8-h period. Without proper ventilation, CO emissions can exceed both the USEPA and OSHA standards for protecting human health. Ethylene and methane play key roles in forming larger VOCs including aromatics such as benzene, toluene, ethylbenzene, and xylene isomers. Sulfur dioxide has many adverse human health effects and could contribute to acid rain. As seen in Figure 9, B40 can clearly provide a greater reduction in the emission of toxicants compared to B20 except for formaldehyde, which shows similar reduction efficiency for B20 and B40 when compared to USLPD. The emission test results supported previous studies showing the reduction of VOCs but there are other studies that reported an increase in hydrocarbon emissions for biodiesel-blended fuels compared to petroleum-based diesel [49].

3.3.2. GC-MS Analysis of VOCs

GC-MS results indicate that there are about 180–200 VOCs detected in the generator emissions. About half of these compounds were detected with a high degree of confidence based on their match indices of greater than 800 out of 1000. There were about 27 target compounds specified in USEPA's Compendium of Air Toxics TO-15 Method that were detected and quantified. Out of the 27 compounds, 11 were quantified with a high degree of confidence for the comparison of generator emissions from ULSPD, B20, and B40. The percent reduction (PR%) values of diesel generator fuel emissions from B20 and B40 relative to ULSPD for these 11 compounds are given in Table S3 in Supplementary Materials. Five of these including benzene, 2-butanone, propene, ethyl benzene and propyl benzene were plotted in Figure 10a,b show a significant reduction of their generator emission concentrations due to the blending of ULSPD with biodiesel. All 11 compounds show lower emissions compared to the ULSPD. Except for two compounds, propene and isopropyl

Energies **2023**, *16*, 5408 16 of 20

alcohol, B40 has higher reduction efficiencies relative to ULSLPD when compared to the B20 emissions.

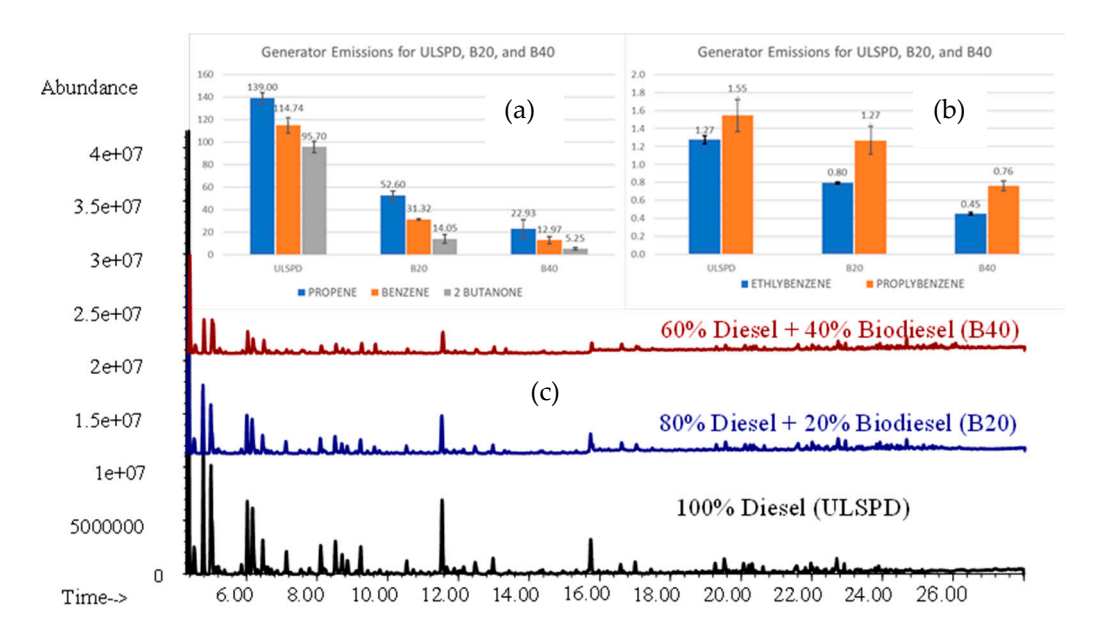


Figure 10. Comparison of GC-MS data for generator emissions from ULSPD, B20, and B40 fuel blends with (a) concentration plots of propene, benzene, and 2-butanone in the range of 0–140 parts per billion (b) concentration plots of ethylbenzene and n-propylbenzene in in the range of 0–2.0 parts per billion, and (c) chromatograms showing significant reduction of volatile organic compounds for B20 and B40 fuel emissions relative to the ULSPD; the X-axis represents the GC retention time window of 4–28 min and the Y-axis denotes the MS ion abundance from 0 to 4×10^7 counts per second with the three plots offset on the common scale.

Three compounds, namely benzene, 1,3-butadiene, and formaldehyde, are classified as Group 1 human carcinogens by the International Agency for Research on Cancer (IARC). At low levels, benzene can cause dizziness, headache, and respiratory tract irritation. However, long-term exposure to higher levels of benzene may cause anemia, alterations to the immune system, and leukemia. OSHA has regulatory standards for PELs and STELs for these three carcinogens and USEPA has detailed information on their toxicological properties in the Integrated Risk Information System (IRIS) database [50]. The Inhalation Unit Risk values of cancer incidence for benzene, 1,3-butadiene, and formaldehyde are $2.2 \times 10^{-6} \text{ per } \mu\text{g/m}^3$, $3 \times 10^{-5} \text{ per } \mu\text{g/m}^3$, and $1.3 \times 10^{-5} \text{ per } \mu\text{g/m}^3$, respectively. At the concentrations indicated in Figure 10c and the conversion factor of 1 μ g/m³ being equal to 0.313 ppbv, 0.452 ppbv, and 0.814 ppbv for the three carcinogens at the standard conditions of 1 atm and 25 °C, respectively, the cancer risks are deemed to be significant for inhalation exposure to diesel generator emissions, especially those from ULSPD. The GC-MS chromatogram in Figure 10c shows an overall decrease in the levels of almost 200 VOCs as the oxygen content of fuel blends increases in the order of ULSPD < B20 < B40, thereby lowering inhalation exposure.

4. Discussion

The results presented in this study are promising for CaO-based heterogeneous catalysts to replace homogeneous catalysts such as NaOH or KOH that are currently used in most commercial biodiesel production facilities. CaO-based catalysts can reduce the need for washing the biodiesel product to remove the residual NaOH that is corrosive to diesel engines. The lower volume of wastewater generation from biodiesel washing is particularly desirable in countries where the use of water for fuel production instead of human consumption is not viewed favorably. This study shows data from multiple instrumentation techniques that the production of CaO catalysts is easy, inexpensive, and

Energies **2023**, 16, 5408 17 of 20

does not generate toxicants harmful to human health. The TGA, FTIR, XRD, and XRF results show that after the calcination of shell materials at 1000 °C for 4 h, all the shell samples containing calcite or CaCO₃ are converted to almost pure CaO powders that give biodiesel yields of greater than 90%.

Although the TGA data show complete conversion of predominantly CaCO₃ into CaO, the FTIR and EDX data show residual CaCO₃ signals which could be interpreted as calcined particles having an outer layer of CaO and an inner core of CaCO₃. Since the sample penetration or signal excitation depths are 1.0–1.5 microns for FTIR and 2.0–2.5 microns for SEM-EDX whereas the CaO crystallites have larger dimensions as revealed by the SEM images, it can be inferred that the particle size distribution and the loading weight in the furnace of uncalcined shell powders in the furnace may influence the degree of calcination or completion CaO formation, and consequently the biodiesel yield and/or the catalyst loading necessary to achieve a high yield. The published studies on the use of CaO catalysts generally do not address their particle size distribution or their correlation with biodiesel yields as well as the durability or reusability of the catalysts. The durability of the CaO catalysts is affected by the dissolution of the surface layer containing Ca(OH)₂ as well as the loss of catalyst active sites through the adsorption or accumulation of oil or biodiesel by-products.

The evaluation of mixed catalysts containing CaO/ZnO seems to suggest that there is no appreciable improvement in biodiesel yields for shell-derived catalysts compared to CaO catalysis except for the case of lobster. It is noteworthy that the SEM-EDX analysis shows the presence of zinc in all the Zn-spiked CaO catalyst samples, but the XRD data only show the presence of distinct ZnO phases at the 10% Zn and 25% Zn mixed oxide samples but not for the 5% Zn and 7% Zn mixed oxide samples. These observations imply that the zinc ion substitution of calcium ions occurred up to a certain point before the distinctive ZnO phases started to form. To confirm this, a future study should rely on the use of elemental mapping by EDX to fully characterize the presence of CaO or ZnO particles and their size distribution.

5. Conclusions

This study demonstrates the feasibility of preparing inexpensive and yet effective heterogeneous CaO catalysts derived from the waste shells of oysters, mussels, lobsters, and chicken eggs. Furthermore, very high biodiesel yields of 90–94% are achieved in 10 min by the ultrasonication-assisted transesterification of canola oil using the CaO catalysts. The incorporation of Zn $^{2+}$ at varying concentrations into the shell-derived CaO structure gives a more efficient CaO-ZnO mixed metal oxide catalyst prepared by the wet impregnation method. The use of CaO-based solid heterogenous catalysts in biodiesel production minimizes wastewater generation for removing residual catalysts in the biodiesel and high energy consumption associated with acid or base homogenous catalysts. The use of shell-based CaO catalysts can also reduce the level of the corrosive base in the biodiesel compared to the commonly used NaOH or KOH catalysts. The use of biodiesel in diesel power generation potentially reduces human exposure to toxicants including CO, SO₂, benzene, and formaldehyde.

Since the shell materials from food waste and furnaces for calcination of shells to yield CaO catalyst are easily available in most countries, the small-scale production of biodiesel is viable in rural areas or developing countries where there is minimal refining capacity to produce diesel fuel for use in vehicles, farm equipment, and power generation. Together with the initiatives to collect used cooking oil and cultivate indigenous crops producing non-edible oils as biodiesel feedstocks, there could be strong incentives to implement a circular economy of producing biodiesel using waste materials and non-edible crops like Jatropha curcas that grow well naturally in many locations.

Energies **2023**, 16, 5408 18 of 20

Supplementary Materials: The following supporting information can be downloaded at: https://www.mdpi.com/article/10.3390/en16145408/s1, Table S1: XRF elemental data for uncalcined and calcined shell samples; Table S2: The American Mineralogist Crystallography Database information for the XRD patterns of oxides in the calcined materials; Table S3: The percent reduction (PR%) values of diesel generator fuel emissions from B20 and B40 relative to ULSPD.

Author Contributions: This manuscript has been prepared using the data and results of the Masters' theses of I.N. and S.A. with additional summer research contribution by D.C. and M.S. The specific contribution of authors is noted as follows. Conceptualization, N.S.C. and B.G.O.; methodology and experimentation, I.N.; formal analysis, I.N., S.A. and N.S.C.; validation, D.C. and M.S.; investigation, N.S.C. and B.G.O.; data curation, M.S.; writing—original draft preparation, I.N. and S.A.; writing—review and editing, N.S.C., B.G.O. and M.S.; visualization, I.N., S.A. and N.S.C.; supervision, N.S.C. and B.G.O.; project administration, N.S.C. and B.G.O.; resources, N.S.C. and B.G.O.; funding acquisition, N.S.C. All authors have read and agreed to the published version of the manuscript.

Funding: This research was partially funded by the National Science Foundation Grant No. 1852543.

Data Availability Statement: The data presented in this study are available in the Supplementary Material.

Acknowledgments: The authors acknowledge the electron microscopy services provided by Joyce Miller, Technical Manager of the MTSU Interdisciplinary Microscopy and Imaging Center.

Conflicts of Interest: The authors declare no conflict of interest. The funding agency had no role in the design of the study; in the collection, analyses, or interpretation of data; in the writing of the manuscript; or in the decision to publish the results.

References

- Wong, K.Y.; Ng, J.-H.; Chong, C.T.; Lam, S.S.; Chong, W.T. Biodiesel Process Intensification through Catalytic Enhancement and Emerging Reactor Designs: A Critical Review. Renew. Sustain. Energy Rev. 2019, 116, 109399. [CrossRef]
- 2. Efavi, J.K.; Kanbogtah, D.; Apalangya, V.; Nyankson, E.; Tiburu, E.K.; Dodoo-Arhin, D.; Onwona-Agyeman, B.; Yaya, A. The Effect of NaOH Catalyst Concentration and Extraction Time on the Yield and Properties of Citrullus Vulgaris Seed Oil as a Potential Biodiesel Feed Stock. S. Afr. J. Chem. Eng. 2018, 25, 98–102. [CrossRef]
- 3. Ling, J.; Tan, Y.; Mujawar, M.; Kansedo, J.; Saptoro, A.; Nolasco-Hipolito, C. A Review of Heterogeneous Calcium Oxide Based Catalyst from Waste for Biodiesel Synthesis. *SN Appl. Sci.* **2019**, *1*, 810. [CrossRef]
- 4. Banerjee, N.; Barman, S.; Saha, G.; Jash, T. Optimization of Process Parameters of Biodiesel Production from Different Kinds of Feedstock. *Mater. Today: Proc.* **2018**, *5*, 23043–23050. [CrossRef]
- 5. Yang, C.; He, K.; Xue, Y.; Li, Y.; Lin, H.; Han, S. Factors Affecting the Cold Flow Properties of Biodiesel: Fatty Acid Esters. *Energy Sources Part A Recovery Util. Environ. Eff.* **2018**, 40, 516–522. [CrossRef]
- 6. Etim, A.O.; Musonge, P.; Eloka-Eboka, A.C. Effectiveness of Biogenic Waste-derived Heterogeneous Catalysts and Feedstock Hybridization Techniques in Biodiesel Production. *Biofuels Bioprod. Bioref.* **2020**, *14*, 620–649. [CrossRef]
- 7. Nayak, S.N.; Bhasin, C.P.; Nayak, M.G. A Review on Microwave-Assisted Transesterification Processes Using Various Catalytic and Non-Catalytic Systems. *Renew. Energy* **2019**, *143*, 1366–1387. [CrossRef]
- 8. Arumugam, A.; Ponnusami, V. Production of Biodiesel by Enzymatic Transesterification of Waste Sardine Oil and Evaluation of Its Engine Performance. *Heliyon* **2017**, *3*, e00486. [CrossRef] [PubMed]
- 9. Van Gerpen, J.; Shanks, B.; Pruszko, R.; Clements, D.; Knothe, G. *Biodiesel Analytical Methods: August 2002–January 2004*; NREL/SR-510-36240; National Renewable Energy Lab. (NREL): Golden, CO, USA, 2004; p. 15008800. [CrossRef]
- 10. Leung, D.Y.C.; Wu, X.; Leung, M.K.H. A Review on Biodiesel Production Using Catalyzed Transesterification. *Appl. Energy* **2010**, 87, 1083–1095. [CrossRef]
- 11. Ashine, F.; Kiflie, Z.; Prabhu, S.V.; Tizazu, B.Z.; Varadharajan, V.; Rajasimman, M.; Joo, S.-W.; Vasseghian, Y.; Jayakumar, M. Biodiesel Production from Argemone Mexicana Oil Using Chicken Eggshell Derived CaO Catalyst. *Fuel* **2023**, 332, 126166. [CrossRef]
- 12. Attari, A.; Abbaszadeh-Mayvan, A.; Taghizadeh-Alisaraei, A. Process Optimization of Ultrasonic-Assisted Biodiesel Production from Waste Cooking Oil Using Waste Chicken Eggshell-Derived CaO as a Green Heterogeneous Catalyst. *Biomass Bioenergy* **2022**, 158, 106357. [CrossRef]
- 13. Mekonnen, K.D.; Sendekie, Z.B. NaOH-Catalyzed Methanolysis Optimization of Biodiesel Synthesis from Desert Date Seed Kernel Oil. *ACS Omega* **2021**, *6*, 24082–24091. [CrossRef]
- 14. Sharma, A.; Kodgire, P.; Kachhwaha, S.S. Investigation of Ultrasound-Assisted KOH and CaO Catalyzed Transesterification for Biodiesel Production from Waste Cotton-Seed Cooking Oil: Process Optimization and Conversion Rate Evaluation. *J. Clean. Prod.* **2020**, 259, 120982. [CrossRef]
- 15. Mishra, V.; Goswami, R. A Review of Production, Properties and Advantages of Biodiesel. Biofuels 2017, 9, 273–289. [CrossRef]

Energies 2023, 16, 5408 19 of 20

16. Singh, D.; Sharma, D.; Soni, S.L.; Sharma, S.; Kumar Sharma, P.; Jhalani, A. A Review on Feedstocks, Production Processes, and Yield for Different Generations of Biodiesel. *Fuel* **2020**, *262*, 116553. [CrossRef]

- 17. El-sherif, A.A.; Hamad, A.M.; Shams-Eldin, E.; Mohamed, H.A.A.E.; Ahmed, A.M.; Mohamed, M.A.; Abdelaziz, Y.S.; Sayed, F.A.-Z.; El Qassem Mahmoud, E.A.A.; Abd El-Daim, T.M.; et al. Power of Recycling Waste Cooking Oil into Biodiesel via Green CaO-Based Eggshells/Ag Heterogeneous Nanocatalyst. *Renew. Energy* 2023, 202, 1412–1423. [CrossRef]
- 18. Chen, G.-Y.; Shan, R.; Yan, B.-B.; Shi, J.-F.; Li, S.-Y.; Liu, C.-Y. Remarkably Enhancing the Biodiesel Yield from Palm Oil upon Abalone Shell-Derived CaO Catalysts Treated by Ethanol. *Fuel Process. Technol.* **2016**, *143*, 110–117. [CrossRef]
- 19. Gaide, I.; Makareviciene, V.; Sendzikiene, E.; Kazancev, K. Snail Shells as a Heterogeneous Catalyst for Biodiesel Fuel Production. *Processes* 2023, 11, 260. [CrossRef]
- 20. Kedir, W.M.; Wondimu, K.T.; Weldegrum, G.S. Optimization and Characterization of Biodiesel from Waste Cooking Oil Using Modified CaO Catalyst Derived from Snail Shell. *Heliyon* **2023**, *9*, e16475. [CrossRef] [PubMed]
- 21. Karkal, S.S.; Rathod, D.R.; Jamadar, A.S.; Mamatha, S.S.; Kudre, T.G. Production Optimization, Scale-up, and Characterization of Biodiesel from Marine Fishmeal Plant Oil Using Portunus Sanguinolentus Crab Shell Derived Heterogeneous Catalyst. *Biocatal. Agric. Biotechnol.* 2023, 47, 102571. [CrossRef]
- 22. Nahas, L.; Dahdah, E.; Aouad, S.; El Khoury, B.; Gennequin, C.; Abi Aad, E.; Estephane, J. Highly Efficient Scallop Seashell-Derived Catalyst for Biodiesel Production from Sunflower and Waste Cooking Oils: Reaction Kinetics and Effect of Calcination Temperature Studies. *Renew. Energy* 2023, 202, 1086–1095. [CrossRef]
- 23. Hangun-Balkir, Y. Green Biodiesel Synthesis Using Waste Shells as Sustainable Catalysts with *Camelina Sativa* Oil. *J. Chem.* **2016**, 2016, 1–10. [CrossRef]
- 24. Nakatani, N.; Takamori, H.; Takeda, K.; Sakugawa, H. Transesterification of Soybean Oil Using Combusted Oyster Shell Waste as a Catalyst. *Bioresour. Technol.* **2009**, *100*, 1510–1513. [CrossRef] [PubMed]
- 25. Aigbodion, V.S. Modified of CaO-Nanoparticle Synthesized from Waste Oyster Shells with Tin Tailings as a Renewable Catalyst for Biodiesel Production from Waste Cooking Oil as a Feedstock. *Chem. Afr.* **2023**, *6*, 1025–1035. [CrossRef]
- 26. Hu, S.; Wang, Y.; Han, H. Utilization of Waste Freshwater Mussel Shell as an Economic Catalyst for Biodiesel Production. *Biomass Bioenergy* **2011**, *35*, 3627–3635. [CrossRef]
- 27. Kumar, D.; Ali, A. Transesterification of Low-Quality Triglycerides over a Zn/CaO Heterogeneous Catalyst: Kinetics and Reusability Studies. *Energy Fuels* **2013**, *27*, 3758–3768. [CrossRef]
- 28. Chong, N.S.; Okejiri, F.U.; Abdulramoni, S.; Perna, S.; Ooi, B.G. Evaluation of Shell-Derived Calcium Oxide Catalysts for the Production of Biodiesel Esters from Cooking Oils. *AJC* **2021**, *6*, 20–27. [CrossRef]
- 29. Chong, N.S.; Abdulramoni, S.; Patterson, D.; Brown, H. Releases of Fire-Derived Contaminants from Polymer Pipes Made of Polyvinyl Chloride. *Toxics* **2019**, *7*, 57. [CrossRef]
- 30. Romano, P.; Fabritius, H.; Raabe, D. The Exoskeleton of the Lobster Homarus Americanus as an Example of a Smart Anisotropic Biological Material. *Acta Biomater.* **2007**, *3*, 301–309. [CrossRef]
- 31. Mergelsberg, S.T.; Ulrich, R.N.; Xiao, S.; Dove, P.M. Composition Systematics in the Exoskeleton of the American Lobster, Homarus Americanus and Implications for Malacostraca. *Front. Earth Sci.* **2019**, 7, 69. [CrossRef]
- 32. Rodriguez-Navarro, C.; Ruiz-Agudo, E.; Luque, A.; Rodriguez-Navarro, A.B.; Ortega-Huertas, M. Thermal Decomposition of Calcite: Mechanisms of Formation and Textural Evolution of CaO Nanocrystals. *Am. Miner.* **2009**, *94*, 578–593. [CrossRef]
- 33. Boßelmann, F.; Romano, P.; Fabritius, H.; Raabe, D.; Epple, M. The Composition of the Exoskeleton of Two Crustacea: The American Lobster Homarus Americanus and the Edible Crab Cancer Pagurus. *Thermochim. Acta* **2007**, *463*, 65–68. [CrossRef]
- 34. Jacobsson, T.J.; Pazoki, M.; Hagfeldt, A.; Edvinsson, T. Goldschmidt's Rules and Strontium Replacement in Lead Halogen Perovskite Solar Cells: Theory and Preliminary Experiments on CH3NH3SrI3. *J. Phys. Chem. C* **2015**, *119*, 25673–25683. [CrossRef]
- 35. Kesić, Ž.; Lukić, I.; Brkić, D.; Rogan, J.; Zdujić, M.; Liu, H.; Skala, D. Mechanochemical Preparation and Characterization of CaO·ZnO Used as Catalyst for Biodiesel Synthesis. *Appl. Catal. A Gen.* **2012**, 427–428, 58–65. [CrossRef]
- 36. Gheisari, H.; Karamian, E.; Abdellahi, M. A Novel Hydroxyapatite –Hardystonite Nanocomposite Ceramic. *Ceram. Int.* **2015**, *41*, 5967–5975. [CrossRef]
- 37. Mohan, K.; Muralisankar, T.; Jayakumar, R.; Rajeevgandhi, C. A Study on Structural Comparisons of α-Chitin Extracted from Marine Crustacean Shell Waste. *Carbohydr. Polym. Technol. Appl.* **2021**, *2*, 100037. [CrossRef]
- 38. Samantaray, S.; Pradhan, D.K.; Hota, G.; Mishra, B.G. Catalytic Application of CeO2–CaO Nanocomposite Oxide Synthesized Using Amorphous Citrate Process toward the Aqueous Phase One Pot Synthesis of 2-Amino-2-Chromenes. *Chem. Eng. J.* **2012**, 193–194, 1–9. [CrossRef]
- 39. Laskar, I.B.; Rajkumari, K.; Gupta, R.; Chatterjee, S.; Paul, B.; Rokhum, S.L. Waste Snail Shell Derived Heterogeneous Catalyst for Biodiesel Production by the Transesterification of Soybean Oil. RSC Adv. 2018, 8, 20131–20142. [CrossRef] [PubMed]
- 40. Dinatha, I.K.H.; Jamilludin, M.A.; Supii, A.I.; Wihadmadyatami, H.; Partini, J.; Yusuf, Y. Characteristics of Bioceramic Hydroxyapatite Based on Sand Lobster Shells (Panulirus Homarus) as Sources of Calcium with Optimal Calcination Temperature. *Mater. Sci. Forum* 2023, 1090, 39–44. [CrossRef]
- 41. Widiarti, N.; Lailun Ni'mah, Y.; Bahruji, H.; Prasetyoko, D. Development of CaO From Natural Calcite as a Heterogeneous Base Catalyst in the Formation of Biodiesel: Review. *J. Renew. Mater.* **2019**, *7*, 915–939. [CrossRef]
- 42. Rizwanul Fattah, I.M.; Ong, H.C.; Mahlia, T.M.I.; Mofijur, M.; Silitonga, A.S.; Rahman, S.M.A.; Ahmad, A. State of the Art of Catalysts for Biodiesel Production. *Front. Energy Res.* **2020**, *8*, 101. [CrossRef]

Energies **2023**, 16, 5408 20 of 20

43. Castro, L.D.S.; Barañano, A.G.; Pinheiro, C.J.G.; Menini, L.; Pinheiro, P.F. Biodiesel Production from Cotton Oil Using Heterogeneous CaO Catalysts from Eggshells Prepared at Different Calcination Temperatures. *Green Process. Synth.* **2019**, *8*, 235–244. [CrossRef]

- 44. Lee, H.; Juan, J.; Yun Hin, T.-Y.; Ong, H. Environment-Friendly Heterogeneous Alkaline-Based Mixed Metal Oxide Catalysts for Biodiesel Production. *Energies* 2016, 9, 611. [CrossRef]
- 45. Kaewdaeng, S.; Sintuya, P.; Nirunsin, R. Biodiesel Production Using Calcium Oxide from River Snail Shell Ash as Catalyst. *Energy Procedia* **2017**, 138, 937–942. [CrossRef]
- Toledo Arana, J.; Torres, J.J.; Acevedo, D.F.; Illanes, C.O.; Ochoa, N.A.; Pagliero, C.L. One-Step Synthesis of CaO-ZnO Efficient Catalyst for Biodiesel Production. Int. J. Chem. Eng. 2019, 2019, 1–7. [CrossRef]
- 47. Awofeso, N. Generator Diesel Exhaust: A Major Hazard to Health and the Environment in Nigeria. *Am. J. Respir. Crit. Care Med.* **2011**, *183*, 1437. [CrossRef] [PubMed]
- 48. "Hot Spots" Stationary Diesel Engine Screening Risk Assessment Tables | California Air Resources Board. Available online: https://ww2.arb.ca.gov/hot-spots-stationary-diesel-engine-screening-risk-assessment-tables (accessed on 28 May 2023).
- 49. Pereira, R.G.; Oliveira, C.D.; Oliveira, J.L.; Oliveira, P.C.P.; Fellows, C.E.; Piamba, O.E. Exhaust Emissions and Electric Energy Generation in a Stationary Engine Using Blends of Diesel and Soybean Biodiesel. *Renew. Energy* 2007, 32, 2453–2460. [CrossRef]
- 50. IRIS Advanced Search. United States Environmental Protection Agency. Available online: https://iris.epa.gov/AdvancedSearch/(accessed on 4 June 2023).

Disclaimer/Publisher's Note: The statements, opinions and data contained in all publications are solely those of the individual author(s) and contributor(s) and not of MDPI and/or the editor(s). MDPI and/or the editor(s) disclaim responsibility for any injury to people or property resulting from any ideas, methods, instructions or products referred to in the content.